MATERIALS PHYSICS AND MECHANICS RESEARCH ARTICLE

Submitted: April 16, 2025 **Revised:** May 3, 2025 **Accepted:** June 3, 2025

Effect of electromagnetic waves on the thermoelastic Hookean unbounded domains based on fractional Fourier law

N. Samir, **M.A. Abdou**, **E. Awad** ✉

Department of Mathematics, Faculty of Education, Alexandria University, Alexandria, Egypt

✉ e-mail: emadawad78@alexu.edu.eg

ABSTRACT

An analytical framework for time-fractional magneto-thermoelasticity in unbounded domains, focusing on heat conduction in materials exhibiting non-classical thermal behavior, are presented. Thermal transport is strongly influenced by temperature and the internal structure of the medium; in the presence of imperfections such as inclusions, voids, or microstructural defects, the heat transfer process often deviates from conventional diffusion laws. To model these complex phenomena, fractional calculus is employed, and the governing equations are reformulated using dimensionless variables. Analytical solution in the Laplace–Fourier domain was derived, with temperature distribution expressed in terms of Mittag-Leffler and Fox H-functions. The use of uncoupled thermoelastic theory allows for a simplified treatment by decoupling thermal and mechanical fields. Finally, numerical inversion techniques are used to reconstruct time-domain solutions for displacement and stress, demonstrating how fractional-order parameters influence both thermal wave propagation and material response.

KEYWORDS

Maxwell's equations • thermoelasticity • fractional derivative • uncoupled theory

Citation: Samir N, Abdou MA, Awad E. Effect of electromagnetic waves on the thermoelastic Hookean unbounded domains based on fractional Fourier law. *Materials Physics and Mechanics*. 2025;53(3): 149–164. http://dx.doi.org/10.18149/MPM.5332025_12

Introduction

In recent decades, the field of thermoelasticity has experienced considerable progress, particularly in efforts to construct a more robust and comprehensive theoretical framework that accurately describes the interplay between thermal and mechanical effects in solid materials. Despite this progress, the conventional or classical formulation of thermoelasticity - commonly referred to as the uncoupled theory - still suffers from two major deficiencies that have long been criticized for their divergence from experimentally observed behavior.

The first critical limitation of the uncoupled thermoelastic theory lies in the way it formulates the heat conduction process. In this classical approach, the governing heat equation is entirely devoid of any terms that account for mechanical or elastic influences. Essentially, the model treats thermal processes as completely independent of mechanical deformations, which is a significant oversimplification of reality. In real-world materials, especially those undergoing rapid or large deformations, temperature changes can both influence and be influenced by the mechanical stresses and strains present within the body. By excluding this coupling, the uncoupled theory fails to capture the intrinsic and complex interdependence between temperature evolution and material deformation, thereby limiting its accuracy and applicability in many practical scenarios. The second major flaw inherent in the traditional uncoupled theory is a mathematical one, rooted in the type of partial differential equation used to describe heat conduction. Specifically, the classical heat equation is parabolic in nature. While this form is mathematically convenient and widely used, it leads to an unphysical prediction: that thermal disturbances - often referred to as "heat waves" - can propagate through a material at infinite speeds. This implication is clearly at odds with empirical evidence and experimental measurements, which have consistently shown that heat propagation in solids occurs at finite velocities. As such, the parabolic character of the classical heat equation undermines the theory's physical realism.

Building upon such foundational ideas, Biot [1] introduced what is now known as the *coupled theory of thermoelasticity*. This theory directly addresses the first shortcoming of the uncoupled model by introducing a mathematical coupling between the equations governing elasticity and those governing heat conduction. In doing so, Biot's formulation allows thermal fields and mechanical fields to influence each other, thereby providing a more realistic and physically consistent description of how materials behave under simultaneous thermal and mechanical loads. However, it is important to note that while Biot's theory successfully overcomes the issue of thermal-mechanical independence, it does not fully resolve the second major concern. Like the uncoupled theory, the coupled theory also employs a parabolic heat equation, and thus still predicts infinite speeds of heat propagation - a result that remains inconsistent with physical reality. Considering these enduring limitations, further theoretical developments have been pursued in the form of *generalized thermoelastic theories*, such as those incorporating hyperbolic heat equations or finite speed models (e.g., the Lord−Shulman and Green−Lindsay theories), which attempt to more accurately reflect the finite speed nature of heat propagation while retaining the essential coupling between thermal and mechanical fields. In an effort to overcome the first major limitation of the classical uncoupled thermoelastic theory - the complete separation between thermal and mechanical responses - Biot [1] introduced what became known as the *coupled theory of thermoelasticity*. This refined model directly links the governing equations of elasticity and heat conduction, thereby eliminating the unrealistic assumption that temperature changes and mechanical deformations occur independently. By integrating these two domains, Biot's theory offered a more realistic representation of material behavior under thermomechanical loads.

Building on the fundamental principles of fractional diffusion-wave equations, researchers have extended these ideas to the realm of thermoelasticity. In [2], for instance, a novel approach to fractional thermoelasticity was introduced, laying the groundwork for further exploration of thermomechanical interactions using fractional calculus. This line of inquiry was first explored in detail by Povstenko, who presented a quasi-static, uncoupled formulation of fractional thermoelasticity. In materials with microstructural irregularities such as voids or impurities, thermal conductivity can exhibit non-classical behavior which motivated the use of fractional-order models. One such approach employs a space-time fractional Fourier law within a quasi-static theory of fractional thermoelasticity to capture anomalous heat conduction effects [3].

At micro- and nanoscales, or under ultrafast thermal excitation, the classical heat conduction model based on Fourier's law becomes inadequate. Its assumption of local thermodynamic equilibrium breaks down under these conditions, leading to inaccurate predictions of thermal behavior. This has driven the development of alternative models that can capture finite thermal propagation speeds and non-equilibrium phenomena. One such alternative is the ballistic-conductive (BC) model, introduced by Kovács and Ván [4] (2015), which extends the classical framework by incorporating both ballistic and diffusive thermal transport mechanisms. While the BC model improves upon the limitations of Fourier's law, analyses of its solutions have revealed a counterintuitive phenomenon: partial "immobilization" of thermal energy. This effect, considered unphysical, highlights the challenges of modeling energy transport in the transition regime between microscopic and macroscopic scales [5].

Moreover, incorporating two-temperature and nonlocal effects into thermoelastic models is essential for accurately predicting material response in ultrafast and nanoscale regimes, where classical thermoelastic theory (based on Fourier's law and instantaneous local equilibrium) fails to capture the true dynamics. To better capture thermal behavior in such regimes, especially during ultrafast processes like laser-material interaction, researchers have turned to two-temperature models. These models separate the electron and phonon subsystems, allowing for local thermal nonequilibrium. Recent extensions to these models introduce time-relaxation and spatial nonlocal effects, enabling more accurate descriptions of thermal transport in metals [6]. Analytical investigations have shown that under high-frequency excitation, key thermal parameters - such as phase velocity, penetration depth, and apparent thermal conductivity - become strongly frequency-dependent. In particular, the apparent thermal conductivity significantly decreases near the characteristic energy exchange frequency between electrons and phonons [7]. This frequency-dependent behavior leads to more complex phenomena such as thermal resonance. Within the framework of the hyperbolic two-temperature model, it has been shown that specific conditions in electron-phonon interactions can result in resonant thermal effects. These findings emphasize the importance of advanced modeling strategies—particularly those that account for microscopic energy exchange mechanisms—in accurately predicting thermal behavior in modern materials [8].

Alongside these developments, fractional-order thermoelastic models have gained attention for their ability to describe anomalous heat conduction and memory effects. For instance, in the context of a semi-infinite medium exposed to a temporally decaying laser pulse, fractional models using Laplace transform techniques have successfully derived temperature, stress, and strain distributions. These solutions, when compared to classical two-temperature models, highlight the advantages of fractional approaches in capturing the subtleties of nonlocal and time-fractional behavior in thermoelastic systems [9].

Complementary to these theoretical advancements, studies have also explored the response of double-porosity materials - complex media with two interacting pore networks - under moving loads. Using Fourier analysis and numerical inversion, researchers have examined the spatial and temporal distributions of stress and temperature, revealing how porosity significantly affects energy dissipation and wave propagation. These findings underscore the importance of microstructural design in determining thermo-mechanical performance under coupled excitations [10].

Building on this understanding of microstructural effects, further studies have investigated systems with layered structures and initial prestress, which introduce additional complexity into the thermoelastic response. In such systems, harmonic thermal excitation leads to intricate coupling between thermal and mechanical fields. Notably, prestress conditions have been shown to alter the pole distribution of the Green function, fundamentally affecting the system's dynamic behavior. This alteration governs wave propagation, energy localization, and the emergence of resonance phenomena within layered media [11].

This paper explores the impact of electromagnetic waves on fractional thermoelastic behavior in unbounded media. In the next section, Maxwell's equations are merged with fractional heat conduction to model the interaction between thermal, elastic and electromagnetic fields. Focusing on a one-dimensional uncoupled system, the goal is to determine the displacement and temperature, linked through hydrostatic stress. The temperature equation is hyperbolic, derived from generalized heat conduction. Using Laplace and Fourier transforms, the PDEs are converted into algebraic equations, solved analytically, and then inverted to retrieve physical solutions. In the "Numerical Analysis and Discussion" sections, we present the final analytical expressions, revealing the influence of material parameters on wave propagation and thermal relaxation.

Mathematical problem

Governing equations

In this sub-section, we will delve into the fundamental equations that govern the behavior of magnetic and electric currents. These equations, collectively known as Maxwell's equations. They describe the relationship between electric and magnetic fields, as well as their interaction with matter. Now we are going to introduce Maxwell's equations as the following [12,13]:

$$\begin{aligned} &\nabla \times E = -\frac{\partial B}{\partial t}, \nabla \times H = J + \frac{\partial D}{\partial t}, \\ &\nabla \cdot D = 0\,, \\ &\nabla \cdot H = 0\,, \end{aligned} \tag{1}$$

where B represents the induced magnetic field which can be expressed as $B = \mu_0 H$ noting that μ_0 stands for the magnetic permeability, H describes the intensity of a magnetic field and J represents the electric current. Additionally, D represents the electric displacement field, which can be expressed as $D = \varepsilon_0 E$, noting that ε_0 represents the electric permeability and E is the electric field intensity. Now we can re-write Eq. (1) as the following:

$$\begin{aligned} &\nabla \times E = -\mu_0 \frac{\partial H}{\partial t}, \nabla \times H = J + \varepsilon_0 \frac{\partial E}{\partial t}, \\ &\nabla \cdot E = 0\,, \\ &\nabla \cdot H = 0\,. \end{aligned} \tag{2}$$

Furthermore, we introduce Ohm's Law that is a fundamental principle in electrical engineering that describes the relationship between voltage, current, and resistance, and we can express Ohm's law as the following [14]:

$$J = \sigma_0 \left(E + \frac{\partial u}{\partial t} \times B \right), \tag{3}$$

where u is the displacement vector, σ_0 is the electric conductivity, and by setting $\sigma_0 \to \infty$ we obtain the perfect conductivity, we also are going to introduce Lorentz force which known as the force experienced by a charged particle moving through an electromagnetic field. The mathematical equation of Lorentz force can be described as the following:

$$\begin{aligned} F &= J \times B, \\ F &= J \times \mu_0(H_0 + h), \end{aligned} \tag{4}$$

where H_0 represents the constant or background magnetic field, it can be thought of as the main steady state magnetic field present in the system. h represents the perturbation or small deviation in the magnetic field caused by external influences and $H_0 + h$ together describes the total magnetic field. Due to the linearity, we can re-write Eq. (4) as the following:

$$F = J \times B_0. \tag{5}$$

The classical theory of thermoelectricity consists of the modified Fourier law mentioned in [15]. By neglecting the electric field intensity $E = 0$ and $h = 0$, so the induced magnetic field becomes $B = \mu_0 H_0$ providing that Eq. (3) becomes as follows:

$$J = \sigma_0 \mu_0 \left(\frac{\partial u}{\partial t} \times H_0 \right). \tag{6}$$

From the unbounded domain configuration, the displacement vector $u = (u, 0,0)$, the electric current vector $J = (0, J, 0)$ and the magnetic field vector $H_0 = (0,0, H_0)$. Consequently, Eq. (6) becomes as the following [16]:

$$J = -\sigma_0 \mu_0 H_0 \frac{\partial u}{\partial t} \underline{j}. \tag{7}$$

Additionally, Eq. (5) becomes the following:

$$F = -\sigma_0 {B_0}^2 \frac{\partial u}{\partial t} \underline{i}. \tag{8}$$

The equation of motion, see [17] after inserting Eq. (8) as an expression for the external force, we obtain the following:

$$\sigma_{ij,j} = \rho \ddot{u}_i + \sigma_0 {B_0}^2 \frac{\partial u_i}{\partial t}. \tag{9}$$

Consequently, by recalling the constitutive relationship presented in [17], as the following:

$$\sigma_{ij} = 2\mu e_{ij} + \lambda e \delta_{ij} - \chi_0 \theta \delta_{ij}, \tag{10}$$

where λ and μ are correspond to the standard Lamé constants, $\theta = T - T_0$ specifically θ is the temperature of the medium, T is the absolute temperature and T_0 is the temperature of the room, $\chi_0 = (3\lambda + 2\mu)\alpha_T$, clarifying that α_T is the parameter that quantifies the linear dimensional change of a material in response to temperature changing or known as the coefficient of linear thermal expansion, σ_{ij} are representing the components of Cauchy stress tensor, δ_{ij} is the Kronecker delta function. And as mentioned above, u_i is the i-th component of displacement vector $\underline{u}$, $e = e_{ii} = u_{i,i} = e_{11} + e_{22} + e_{33}$ is known as the cubical dilation and e_{ij} is representing the strain tensor for linear elasticity defined that is define as: $e_{ij} = \frac{1}{2}(u_{i,j} + u_{j,i})$.

Now, the well-known stress-strain relation, see [18] can be modified by inserting Eq. (9) as the following:

$$\mu u_{i,jj} + (\lambda + \mu) u_{j,ij} - \chi_0 T_{,i} = \rho \ddot{u}_i + \sigma_0 {B_0}^2 \frac{\partial u_i}{\partial t}. \tag{11}$$

At this stage, we will reintroduce the thermal energy balance equation in the absence of a heat source in one dimension setting as the following [19]:

$$-q_{i.i} = \rho C_E \dot{T} + \chi_0 T_0 \dot{e}. \tag{12}$$

where $\dot{e} = \frac{\partial^2 u}{\partial x \partial t}$. Additionally, it's important to revisit the core concept of heat conduction known as Fourier's law. This principle states that the heat flux—defined as the amount of heat energy transferred per unit area per unit time—is directly proportional to the temperature gradient, which describes how temperature changes over distance. In mathematical terms, Fourier's law is written as [20,21]: $q_i = -\kappa T_{,i}$. We will adopt an alternative rule that will serve as the foundation for our proceeding analysis, offering a more understanding of heat transfer phenomena under a given conditions as follows:

$$q_i = -\kappa_\alpha {}_{0}^{RL}\mathcal{D}_t^{1-\alpha} T_{,i}. \tag{13}$$

The operator ${}_{a^+}^{RL}\mathcal{D}_t^{\alpha}$ denotes the left-sided Riemann-Liouville fractional derivative, which is defined for a general function, further details can be found in [22-24]. Building upon the insightful proposition by Compte and Metzler concerning the anomalous diffusion coefficient, we propose the following functional expressions for the parameter κ_α:

$$\kappa_\alpha = \kappa \tau^{1-\alpha}, \tag{14}$$

where κ is the classical thermal conductivity, τ is a characteristic time constant. τ will be specified subsequently. Equation (14) becomes as the following:

$$q_i = -\kappa \tau^{1-\alpha} {}_{0}^{RL}\mathcal{D}_t^{1-\alpha} T_{,i}. \tag{15}$$

To streamline our analysis, we will eliminate the heat flux term that appears in both the energy balance equation (12) and Eq. (15). This will be achieved by employing a suitable mathematical technique, as outlined below:

$$\rho C_E \dot{T} + \chi_0 T_0 \, \dot{e} = \kappa \tau^{1-\alpha} {}_{0}^{RL}\mathcal{D}_t^{1-\alpha} T_{,ii} \, . \tag{16}$$

Problem setting up

In this section, we will develop a mathematical framework to describe the system outlined in Eqs. (11) and (16). This system is defined over an unbounded spatial domain $-\infty < x < \infty$, signifying that it extends infinitely in all directions. To establish a complete mathematical description, we must specify the initial conditions that govern the system's behavior. These initial conditions will serve as the starting point for our analysis and will significantly influence the subsequent evolution of the system. The initial conditions are given as follows:

$$\theta(x,0) = \vartheta_0 \delta(x), \;\; u(x,0) = \frac{\partial u(x,0)}{\partial x} = 0, \tag{17}$$

where $\delta(x)$ is the Dirac delta function assuming that the displacement initial state is given as $u(-\infty,0) = u_{-\infty}$. By noticing the initial conditions outlined in Eq. (17), we observe that the complexity of the problem can be significantly reduced to a one-dimensional framework. This simplification arises due to the inherent nature of the initial state, which exhibits a particular symmetry that allows us to focus our analysis along a single spatial dimension. This means that all relevant physical quantities involved in the problem can be expressed as functions of the spatial variable x (one-dimensional setting) and time t. Consequently, the governing equations, represented by Eqs. (11) and (16), can be simplified to involve only derivatives with respect to these two independent variables, x and t. This reduction in dimensionality significantly simplifies the mathematical analysis and allows for more efficient numerical simulations. The simplified governing equations are as follows:

$$(\lambda + 2\mu) \frac{\partial^2 u}{\partial x^2} - \chi_0 \frac{\partial T}{\partial x} = \rho \ddot{u} + \sigma_0 {B_0}^2 \frac{\partial u}{\partial t}, \tag{18}$$

$$\rho C_E \frac{\partial T}{\partial t} + \chi_0 T_0 \frac{\partial^2 u}{\partial x \partial t} = \kappa \tau^{1-\alpha}\, {}^{RL}_{0}\mathcal{D}_t^{1-\alpha} \frac{\partial^2 T}{\partial x^2}. \tag{19}$$

By employing Eq. (10) together with the previously established one-dimensional framework, the individual components of the Cauchy stress tensor can be explicitly calculated using the following procedure:

$$\sigma_{xx} = (\lambda + 2\mu)\frac{\partial u}{\partial x} - \chi_0 (T - T_0), \tag{20}$$

$$\sigma_{yy} = \sigma_{zz} = \lambda \frac{\partial u}{\partial x} - \chi_0 (T - T_0). \tag{21}$$

In the context of hydrostatic stress σ_H, we focus solely on the normal components. By taking their arithmetic means, we obtain a single value that characterizes the overall pressure exerted on the material from all directions. This average pressure is what we refer to as hydrostatic stress:

$$\sigma_H = \frac{\sigma_{xx}+\sigma_{yy}+\sigma_{zz}}{3} = \left(\lambda + \frac{2}{3}\mu\right)\frac{\partial u}{\partial x} - \chi_0 (T - T_0). \tag{22}$$

To facilitate a more comprehensive and insightful analysis of the problem, we will introduce a set of dimensionless variables. By systematically reducing the number of independent parameters, we can significantly streamline the mathematical model, simplifying its interpretation and analytical processing as detailed below:

$$\begin{gathered} x \to \frac{x}{c_1 \eta}, \quad u \to \frac{u}{c_1 \eta}, t \to \frac{t}{c_1^2 \eta}, \\ \tau \to \frac{\tau}{c_1^2 \eta}, \quad (\sigma_{ij}, \sigma_H) \to (\lambda + 2\mu)(\sigma_{ij}, \sigma_H), \eta = \frac{\rho C_E}{\kappa}, \\ T \to \frac{\lambda+2\mu}{\chi_0}\theta + T_0, c_1^2 = \frac{\lambda+2\mu}{\rho}, \end{gathered} \tag{23}$$

therefore, the governing equations (18) and (19) can be rewritten as the following:

$$\frac{\partial \theta}{\partial x} = \frac{\partial^2 u}{\partial x^2} - \frac{\partial^2 u}{\partial t^2} - c_0 \frac{\partial u}{\partial t}, \tag{24}$$

where

$$\begin{gathered} c_0 = \frac{\sigma_0 {B_0}^2}{\eta(\lambda+2\mu)}, \\ \frac{\partial \theta}{\partial t} + \varepsilon \frac{\partial^2 u}{\partial x \partial t} = \tau^{1-\alpha}\, {}^{RL}_{0}\mathcal{D}_t^{1-\alpha} \frac{\partial^2 \theta}{\partial x^2}, \end{gathered} \tag{25}$$

where ε is the thermoelastic coupling constant and given as the following: $\varepsilon = \frac{{\chi_0}^2 T_0}{\rho C_E (\lambda+2\mu)}$.

Additionally, the constitutive relations (20)–(22) can be also rewritten in the dimensionless form as the following:

$$\begin{gathered} \sigma_{xx} = \frac{\partial u}{\partial x} - \theta, \\ \sigma_{yy} = \sigma_{zz} = \ell_0 \frac{\partial u}{\partial x} - \theta, \end{gathered} \tag{26}$$

where $\ell_0 = \frac{\lambda}{\lambda+2\mu}$.

Additionally,

$$\sigma_H = \ell_1 \frac{\partial u}{\partial x} - \theta, \tag{27}$$

where $\ell_1 = \frac{(\lambda+\frac{2}{3}\mu)}{(\lambda+2\mu)}$.

Now, we are going to use the dimensionless variable on the initial condition as previously outlined in Eq. (17) as the following:

$$\begin{gathered} \theta(x,0) = \Theta_0 \delta(x), \\ u(x,0) = \frac{\partial u(x,0)}{\partial x} = 0 \text{ and } u(-\infty,0) = U_{-\infty}, \end{gathered} \tag{28}$$

where $\Theta_0 = \frac{\chi_0 \vartheta_0 c_1 \eta}{\lambda+2\mu}$, noting that the dimensions of Dirac delta function $\delta(x)$ in our context must be the inverse of the dimensions of x.

Solution in the transformed domain

In the subsequent analysis, we will embark on deriving an analytical solution for the temperature field within the Laplace-Fourier domain. This certain mathematical approach will enable us to delve deeper into the fundamental behavior of heat transfer within the system.

To proceed, we will apply the Laplace transform on Eq. (24), as detailed below:

$$\frac{\partial\tilde{\theta}}{\partial x}=\frac{\partial^2\tilde{u}}{\partial x^2}-s^2\tilde{u}-c_0 s\tilde{u}, \tag{29}$$

by differentiating Eq. (29) with respect to x, we get the following:

$$\frac{\partial^2\tilde{\theta}}{\partial x^2}=\frac{\partial^2\tilde{e}}{\partial x^2}-s^2\tilde{e}-c_0 s\tilde{e}. \tag{30}$$

Now, to further our analysis, we proceed by applying the Fourier transform to Eq. (30). This mathematical operation will enable us to facilitate the subsequent analysis and solution of the equation as the following:

$$-\omega^2\hat{\tilde{\theta}}=-\omega^2\hat{\tilde{e}}-s^2\hat{\tilde{e}}-c_0 s\hat{\tilde{e}}. \tag{31}$$

Consequently, we apply the Laplace transform to Eq. (25), resulting in the following transformed equation:

$$s\tilde{\theta}-\Theta_0\delta(x)+\varepsilon s\tilde{e}=\tau^{1-\alpha}s^{1-\alpha}\frac{\partial^2\tilde{\theta}}{\partial x^2}. \tag{32}$$

To initiate our analysis, we employ the uncoupled theory of thermoelasticity by setting $\varepsilon=0$, a simplified approach that decouples the thermal and mechanical fields. This theory assumes that mechanical deformations have a negligible influence on the temperature distribution. In other words, changes in temperature do not influence the mechanical deformation, and vice versa. Meaning that the heat conduction equation is solved independently and the effect of mechanical deformation on heat conduction is considered negligible [25].

Therefore, after applying Fourier transform on Eq. (32) which allows us to analyze the equation and get an expression for $\hat{\tilde{\theta}}(\omega,s)$ as the following:

$$\hat{\tilde{\theta}}(\omega,s)=\left(\frac{\Theta_0\tau^{\alpha-1}s^{\alpha-1}}{\tau^{\alpha-1}s^{\alpha}+\omega^2}\right). \tag{33}$$

We proceed by applying the rule of Fourier inverse transformation mentioned in [26] on Eq. (33) as follows: $\mathcal{F}^{-1}\left\{\frac{1}{\omega^2+c^2}\right\}=\frac{1}{2c}e^{-c|x|}$. Therefore:

$$\tilde{\theta}(x,s)=\frac{\Theta_0\sqrt{\tau^{\alpha-1}s^{\alpha-2}}}{2}\exp\left(-\sqrt{\tau^{\alpha-1}s^{\alpha}}|x|\right). \tag{34}$$

And subsequently, by simplifying and performing the technique of partial fraction decomposition to further simplify Eq. (31), we obtain an expression for $\hat{\tilde{e}}(\omega,s)$ as the following:

$$\hat{\tilde{e}}(\omega,s)=\frac{\Theta_0\tau^{\alpha-1}s^{\alpha-1}}{\tau^{\alpha-1}s^{\alpha}-s^2-c_0 s}\left(\frac{-(s^2+c_0 s)}{\omega^2+s^2+c_0 s}+\frac{\tau^{\alpha-1}s^{\alpha}}{\omega^2+\tau^{\alpha-1}s^{\alpha}}\right). \tag{35}$$

Within the following discussion, we are going to calculate the temperature within the material. Starting by reformulating Eq. (33) to convert the temperature function from the Laplace domain, characterized by the complex variable s, back to the time domain, characterized by the real variable t, we employ the inverse Laplace transform as follows [27]:

$$\tilde{\theta}(\omega,t)=\mathcal{L}^{-1}\left\{\frac{\Theta_0 s^{\alpha-1}}{s^{\alpha}+\omega^2\tau^{1-\alpha}}\right\}=\Theta_0 E_{\alpha}\left(-\omega^2\tau^{1-\alpha}t^{\alpha}\right), \tag{36}$$

where the symbol $E_\alpha(\cdot)$ denotes the Mittag-Leffler function with one parameter α, see reference [28] for more details. By applying the inverse Fourier transform to Eq. (36), referencing the relationships (A.10) and (A.20) in [18], we can derive a closed-form expression for temperature, as follows:

$$\tilde{\theta}(\omega,t) = \Theta_0 H_{1,2}^{1,1}\left[\omega^2\tau^{1-\alpha}t^\alpha \middle| \begin{matrix}(0,1)\\(0,1),(0,\alpha)\end{matrix}\right]. \tag{37}$$

Upon applying the inverse Fourier transformation to Eq. (37), we arrive at the following outcome:

$$\theta(x,t) = \frac{\Theta_0}{\sqrt{4\pi}}\left(\frac{1}{\tau^{1-\alpha}t^\alpha}\right)^{\frac{1}{2}} \times H_{2,3}^{2,1}\left[\frac{x^2}{2^2\tau^{1-\alpha}t^\alpha}\middle| \begin{matrix}\left(\frac{1}{2},1\right);\left(1-\frac{\alpha}{2},\alpha\right)\\(0,1),\left(\frac{1}{2},1\right);\left(\frac{1}{2},1\right)\end{matrix}\right]. \tag{38}$$

The symbol $H_{p,q}^{m,n}[\cdot]$ represents the Fox H-function, a mathematical function defined in terms of the Mellin-Barnes integral, as outlined in reference [29] and. When examining the solution represented by Eq. (38), we notice that the closed-form expression of this solution can be modified or transformed. The objective of the following analysis is to determine the analytical solution for $\hat{\hat{e}}(\omega,s)$, while numerical integration techniques can provide approximate solutions. To proceed with the analysis, we will apply the following inverse Fourier transform to Eq. (35) [26]:

$$\begin{aligned}\tilde{e}(x,s) = \frac{\Theta_0\tau^{\alpha-1}s^{\alpha-1}}{\tau^{\alpha-1}s^\alpha - s^2 - c_0 s} \times \Bigg(\frac{-(s^2+c_0 s)^{\frac{1}{2}}}{2}\exp\left(-(s^2+c_0 s)^{\frac{1}{2}}|x|\right) + \\ + \frac{(\tau^{\alpha-1}s^\alpha)^{\frac{1}{2}}}{2}\exp\left(-(\tau^{\alpha-1}s^\alpha)^{\frac{1}{2}}|x|\right)\Bigg).\end{aligned} \tag{39}$$

To determine the displacement, we perform an integration of Eq. (39) with respect to the spatial variable x. This approach is based on the relationship given by $e = \frac{\partial u}{\partial x}$:

$$\tilde{u}(x,s) = \tilde{u}(-\infty,s) + \frac{\Theta_0\tau^{\alpha-1}s^{\alpha-1}}{2\tau^{\alpha-1}s^\alpha - s^2 - c_0 s}(I_1 + I_2), \tag{40}$$

recalling that $\tilde{u}(-\infty,s) = \frac{U_{-\infty}}{s}$, $I_1 = -(s^2+c_0 s)^{\frac{1}{2}}\int_{-\infty}^{x} e^{-(s^2+c_0 s)^{\frac{1}{2}}|\xi|}d\xi$, $I_2 = (\tau^{\alpha-1}s^\alpha)^{\frac{1}{2}}\int_{-\infty}^{x} e^{-(\tau^{\alpha-1}s^\alpha)^{\frac{1}{2}}|\xi|}d\xi$ based on the sign of x. Specifically, when $x > 0$, the absolute value simplifies to $|x| = x$, while for $x < 0$, the absolute value becomes $|x| = -x$. To proceed systematically, we first analyze the case where $x > 0$. Under this condition, the first and second integrals are reformulated accordingly, and their expressions are derived as follows:

$$I_1 = -(s^2+c_0 s)^{\frac{1}{2}}\left(\int_{-\infty}^{0} e^{-(s^2+c_0 s)^{\frac{1}{2}}|\xi|}d\xi + \int_{0}^{x} e^{-(s^2+c_0 s)^{\frac{1}{2}}|\xi|}d\xi\right), \tag{41}$$

by replacing $\xi = -X$ therefore $d\xi = -dX$ into the first part of integral (41) as:

$$\begin{aligned}I_1 &= -(s^2+c_0 s)^{\frac{1}{2}}\left(\int_{0}^{\infty} e^{-(s^2+c_0 s)^{\frac{1}{2}}X}dX + \int_{0}^{x} e^{-(s^2+c_0 s)^{\frac{1}{2}}\xi}d\xi\right), \\ I_1 &= e^{-(s^2+c_0 s)^{\frac{1}{2}}x} - 2.\end{aligned} \tag{42}$$

And similarly for I_2:

$$\begin{aligned}I_2 &= (\tau^{\alpha-1}s^\alpha)^{\frac{1}{2}}\left(\int_{-\infty}^{0} e^{-(\tau^{\alpha-1}s^\alpha)^{\frac{1}{2}}|\xi|}d\xi + \int_{0}^{x} e^{-(\tau^{\alpha-1}s^\alpha)^{\frac{1}{2}}|\xi|}d\xi\right) = \\ &= (\tau^{\alpha-1}s^\alpha)^{\frac{1}{2}}\left(\int_{0}^{\infty} e^{-(\tau^{\alpha-1}s^\alpha)^{\frac{1}{2}}X}dX + + \int_{0}^{x} e^{-(\tau^{\alpha-1}s^\alpha)^{\frac{1}{2}}\xi}d\xi\right) = 2 - e^{-(\tau^{\alpha-1}s^\alpha)^{\frac{1}{2}}x}.\end{aligned} \tag{43}$$

Therefore, in case of $x > 0$ the displacement $\tilde{u}(x,s)$ is given by employing Eqs. (42) and (43) into Eq. (40) as the following:

$$\tilde{u}(x,s) = \frac{U_{-\infty}}{s} + \frac{\Theta_0 \tau^{\alpha-1} s^{\alpha-1}}{2\tau^{\alpha-1}s^{\alpha} - s^2 - c_0 s}\left(e^{-(s^2+c_0 s)^{\frac{1}{2}}x} - e^{-(\tau^{\alpha-1}s^{\alpha})^{\frac{1}{2}}x}\right), \quad x > 0. \tag{44}$$

Subsequently, we examine the second case, where $x < 0$, and incorporate this condition into the evaluation of the first and second integrals, denoted as I_1 and I_2 as the following:

$$I_1 = -(s^2 + c_0 s)^{\frac{1}{2}}\left(\int_{-\infty}^{0} e^{-(s^2+c_0 s)^{\frac{1}{2}}|\xi|} d\xi - \int_{x}^{0} e^{-(s^2+c_0 s)^{\frac{1}{2}}|\xi|} d\xi\right), \tag{45}$$

by replacing $\xi = -X$ therefore $d\xi = -dX$ into integral Eq. (45) as:

$$I_1 = -(s^2 + c_0 s)^{\frac{1}{2}}\left(\int_{0}^{\infty} e^{-(s^2+c_0 s)^{\frac{1}{2}}X} dX + \int_{-x}^{0} e^{-(s^2+c_0 s)^{\frac{1}{2}}X} dX\right) = -e^{(s^2+c_0 s)^{\frac{1}{2}}x}.$$

And similarly, for I_2:

$$\begin{aligned} I_2 &= (\tau^{\alpha-1}s^{\alpha})^{\frac{1}{2}}\left(\int_{-\infty}^{0} e^{-(\tau^{\alpha-1}s^{\alpha})^{\frac{1}{2}}|\xi|} d\xi - \int_{x}^{0} e^{-(\tau^{\alpha-1}s^{\alpha})^{\frac{1}{2}}|\xi|} d\xi\right) = \\ &= (\tau^{\alpha-1}s^{\alpha})^{\frac{1}{2}}\left(\int_{0}^{\infty} e^{-(\tau^{\alpha-1}s^{\alpha})^{\frac{1}{2}}X} dX + + \int_{-x}^{0} e^{-(\tau^{\alpha-1}s^{\alpha})^{\frac{1}{2}}X} dX\right) = e^{(\tau^{\alpha-1}s^{\alpha})^{\frac{1}{2}}x}. \end{aligned} \tag{46}$$

Therefore, in case of $x < 0$ the displacement $\tilde{u}(x,s)$ is given by employing Eqs. (45) and (46) into Eq. (40) as the following:

$$\tilde{u}(x,s) = \frac{U_{-\infty}}{s} + \frac{\Theta_0 \tau^{\alpha-1} s^{\alpha-1}}{2\tau^{\alpha-1}s^{\alpha} - s^2 - c_0 s}\left(e^{(\tau^{\alpha-1}s^{\alpha})^{\frac{1}{2}}x} - e^{(s^2+c_0 s)^{\frac{1}{2}}x}\right), \quad x < 0. \tag{47}$$

By considering the contributions from all relevant components or elements, the displacement in the Laplace domain can be expressed collectively in the following form:

$$\tilde{u}(x,s) = \frac{U_{-\infty}}{s} + \frac{\Theta_0 \tau^{\alpha-1} s^{\alpha-1}}{2\tau^{\alpha-1}s^{\alpha} - s^2 - c_0 s}\begin{cases} e^{-(s^2+c_0 s)^{\frac{1}{2}}x} - e^{-(\tau^{\alpha-1}s^{\alpha})^{\frac{1}{2}}x}, & x > 0, \\ e^{(\tau^{\alpha-1}s^{\alpha})^{\frac{1}{2}}x} - e^{(s^2+c_0 s)^{\frac{1}{2}}x}, & x < 0. \end{cases} \tag{48}$$

To determine the hydrostatic stress in the Laplace domain, we formulate the expression as follows:

$$\widetilde{\sigma_H} = \ell_1 \frac{\partial \tilde{u}}{\partial x} - \tilde{\theta}. \tag{49}$$

At this stage, we proceed by substituting the appropriate expressions from Eqs. (34) and (48) into the previous formulation Eq. (49) as follows:

$$\begin{aligned} \widetilde{\sigma_H} &= \ell_1 \frac{\partial}{\partial x}\left(\frac{U_{-\infty}}{s} + \frac{\Theta_0 \tau^{\alpha-1} s^{\alpha-1}}{2\tau^{\alpha-1}s^{\alpha} - s^2 - c_0 s}\begin{cases} e^{-(s^2+c_0 s)^{\frac{1}{2}}x} - e^{-(\tau^{\alpha-1}s^{\alpha})^{\frac{1}{2}}x}, & x > 0 \\ e^{(\tau^{\alpha-1}s^{\alpha})^{\frac{1}{2}}x} - e^{(s^2+c_0 s)^{\frac{1}{2}}x}, & x < 0 \end{cases}\right) - \\ &- \left(\frac{\Theta_0 \sqrt{\tau^{\alpha-1}s^{\alpha-2}}}{2} e^{-\sqrt{\tau^{\alpha-1}s^{\alpha}}|x|}\right). \end{aligned} \tag{50}$$

Numerical analysis and Discussion

In this section, we reconstruct the solutions for displacement and hydrostatic stress in the physical domain using a suitable numerical technique. One of the most effective methods for inverting the Laplace transform is the application of the "Durbin" method or the "modified Dubner–Abate" formula [30].

$$f(x,t) = \frac{2e^{at}}{T_1}\left\{-\frac{1}{2}\tilde{f}(x,a) + \Re\left[\sum_{k=0}^{\text{NSum}} \tilde{f}\left(x, a+\frac{2\pi lk}{T_1}\right) cos\left(\frac{2\pi kt}{T_1}\right)\right] - \right.$$
$$\left. -\Im\left[\sum_{k=0}^{\text{NSum}} \tilde{f}\left(x, a++\frac{2\pi lk}{T_1}\right) sin\left(\frac{2\pi kt}{T_1}\right)\right]\right\}, \tag{51}$$

where the parameter T_1 satisfies the inequality $0 < t \leq 2T_1$. The number of summed terms, represented as NSum, typically ranges from 10^5 for small time values to 10^7 for larger ones. values of time to yield stable results with negligible error given by the following:

$$\text{ERROR}(a, t, T_1) = \sum_{k=1}^{\infty} e^{-2akT_1}\tilde{f}(x, 2kT_1 + t). \tag{52}$$

The implementation of series (51) can be carried out using an appropriate symbolic computation software. Programs such as MATHCAD or MATLAB provide powerful tools for handling symbolic calculations. On the other hand and before implementing the previous series, we have obtained an exact solution for the temperature in Eq. (38), which can be computed by the series expansion of the Fox H-function [29] as the following steps:

$$\theta(x,t) = \frac{\Theta_0}{\sqrt{4\pi}}\left(\frac{1}{\tau^{1-\alpha}t^{\alpha}}\right)^{\frac{1}{2}}\{\theta_1(x,t) + \theta_2(x,t)\}, \tag{53}$$

to obtain $\theta_1(x,t)$, we are going to use $b_h = b_1 = 0$, $B_h = B_1 = 1$ and $\frac{b_1+\nu}{B_1} = \nu$, then we get the following:

$$\theta_1(x,t) = \sum_{\nu=0}^{\infty}\frac{(-1)^{\nu}}{\nu!}\left(\frac{|x|^2}{2^2\tau^{1-\alpha}t^{\alpha}}\right)^{\nu}\frac{\Gamma\left(\frac{1}{2}-\nu\right)\Gamma\left(\frac{1}{2}+\nu\right)}{\Gamma\left(\frac{1}{2}+\nu\right)\Gamma\left(1-\frac{\alpha}{2}-\alpha\nu\right)}. \tag{54}$$

Similarly, for $\theta_2(x,t)$ we use $b_h = b_2 = \frac{1}{2}$, $B_h = B_2 = 1$ and $\frac{b_2+\nu}{B_2} = \frac{1}{2} + \nu$, then we get the following:

$$\theta_2(x,t) = \sum_{\nu=0}^{\infty}\frac{(-1)^{\nu}}{\nu!}\left(\frac{|x|^2}{2^2\tau^{1-\alpha}t^{\alpha}}\right)^{\frac{1}{2}+\nu}\frac{\Gamma\left(\frac{1}{2}-(1+\nu)\right)\Gamma(1+\nu)}{\Gamma((1+\nu))\Gamma(1-\alpha(1+\nu))}. \tag{55}$$

For our numerical computations, we have chosen copper to be our material. We will use its physical properties measured at room temperature (300 K) in our mathematical models to simulate its behavior under various conditions. Since $\tau = 1/c_1^2\eta$, the dimensional characteristic constant τ is selected such that the dimensionless constant in all closed-form expressions and their series expansions equals one. Unless explicitly stated otherwise, we will adopt the following specific values for the material properties in our calculations. These values will serve as the standard parameters for the material unless alternative data is provided.

$$\alpha = 1, \tau = 0.01, \;\; \Theta_0 = 1, \; c_0 = 4.36d - 4\,. \tag{56}$$

Equations (53)–(55) serve as the mathematical formulas directly applied in a numerical technique to compute the temperature. The infinite series within these formulae were approximated by summing the first seventy-one terms. Utilizing their series representation, we visually illustrate the temperature distribution in Fig. 1, that clearly demonstrates that the magnetic field has no influence on temperature, as there is no coupling between the two; $\varepsilon_0 = 0$. In Fig. 1, the temperature distribution is evaluated for different values of α, at $\alpha = 1$ the curve leads to the normal distribution. Varying α reveals the impact of anomalous thermal conductivity. Specifically, for smaller values of α, the system exhibits low thermal conductivity, whereas larger values of α correspond to higher thermal conductivity, leading to a wider temperature distribution within the medium.

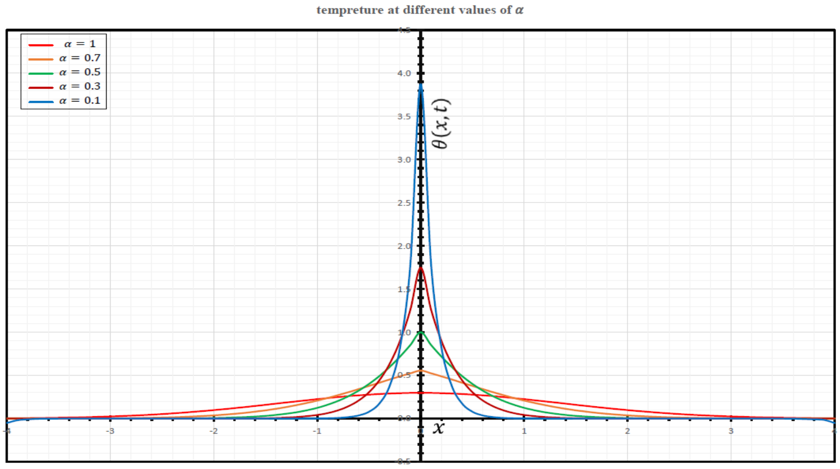

Fig. 1. The temperature distribution evaluated for different values of α

Figure 2 shows the fractional-order parameter α fixed at a representative value of 0.5, while the temperature distribution is analyzed at multiple time instances: $t = 0.1, 0.5, 1, 5$ and 10. Initially, the temperature exhibits a sharp peak near the origin due to the localized thermal disturbance. As time progresses, the peak diminishes and the distribution extends symmetrically, reflecting the diffusion of heat through the medium. This approach allows for the understanding of the temporal evolution of thermal propagation under anomalous heat conduction conditions. The observed behavior shows the effect of time on the diffusion of thermal energy in a medium governed by non-classical (fractional) thermal conductivity, where heat spreads more gradually and the profile undergoes significant changes in shape as time progresses.

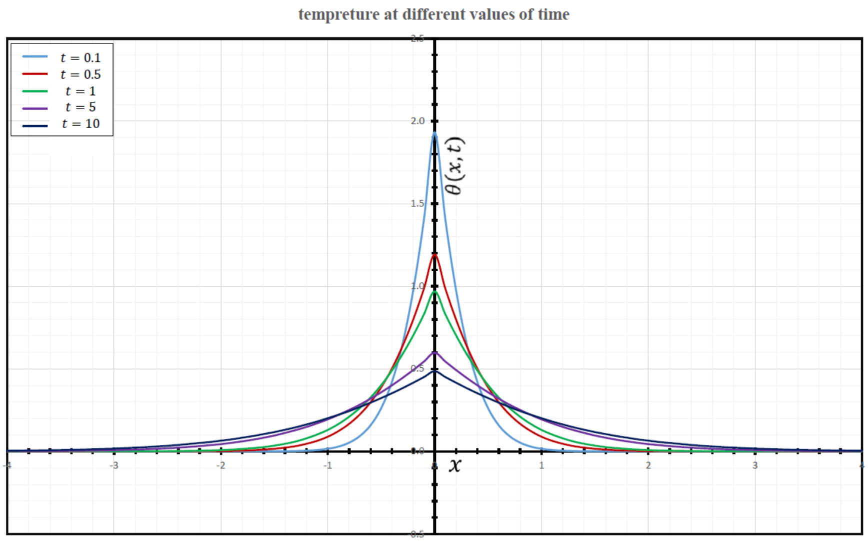

Fig. 2. The temperature distribution for various time instances t, illustrating the temporal evolution of the thermal field

In Fig. 3, the displacement field $u(x,t)$ is presented for $t = 1$ and various values of the fractional parameter α, showing the impact of anomalous thermal conductivity on the mechanical response. As α decreases, the displacement profile becomes sharper and more localized, indicating stronger non-local effects and delayed thermal diffusion. This behavior indicates a significant limitation of thermal diffusion, resulting in a reduced and more constrained mechanical response. Consequently, the displacement field tends to freeze. In contrast, under normal (classical) thermal conduction, the thermal energy propagates more rapidly through the medium, leading to a broader and more extended displacement profile over space and time. This demonstrates the influence of fractional-order behavior on the deformation characteristics of the material, while Fig. 4 represents the displacement at $\alpha = 0.5$ and different values of time $t = 0.1, 0.5, 1, 5$ and 10. The results demonstrate that, as time increases, the displacement propagates and smoothens, showing the diffusive nature of the underlying thermoelastic response. The observed behavior also emphasizes the time-dependent influence of anomalous thermal conductivity on the mechanical response of the medium.

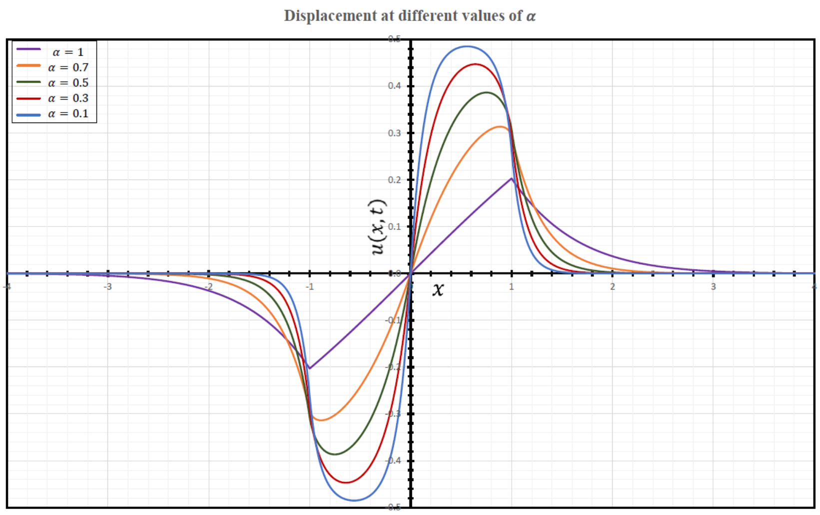

Fig. 3. As the thermal conductivity decreases—represented by lower values of the fractional parameter α is the displacement profile becomes increasingly localized and exhibits sharper curvature near the origin

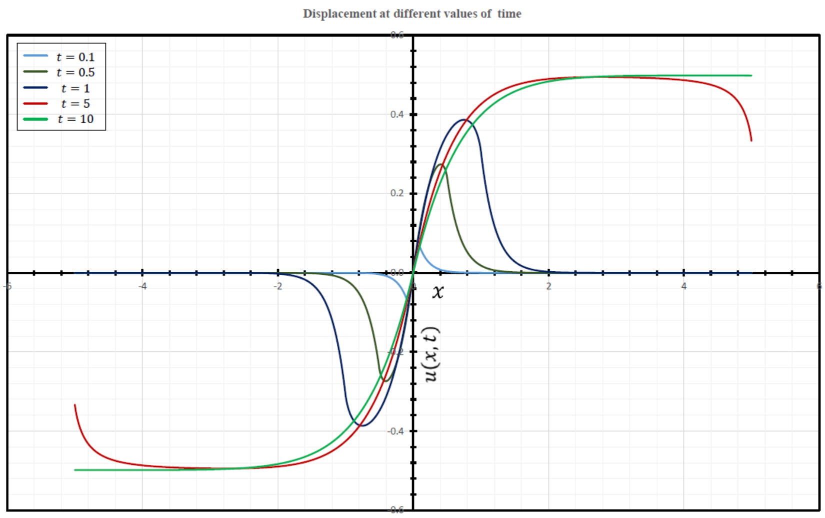

Fig. 4. The spatial profile of the displacement $u(x,t)$ illustrated for various values of time t, highlighting the temporal evolution of the displacement field

Figure 5 represents the hydrostatic stress at $t = 1$ and different values of α which reveal a significant role of the fractional-order parameter in governing the thermoelastic behavior of the material. As α decreases, corresponding to stronger anomalous diffusion effects, the stress profiles exhibit sharper gradients and deeper dips. This indicates an intense stress concentration. Figure 6 demonstrates the temporal evolution of the stress field, as time progresses, the stress profile becomes increasingly, well-defined and exhibits greater symmetry about the origin, with the peak values shifting spatially and magnifying in magnitude. The results show that, over time, the stress profile becomes clearer and more symmetric around the origin, with peak magnitudes shifting and deepening. This behavior reflects the dynamic coupling between thermal diffusion and mechanical deformation, further influenced by the anomalous heat conduction mechanism.

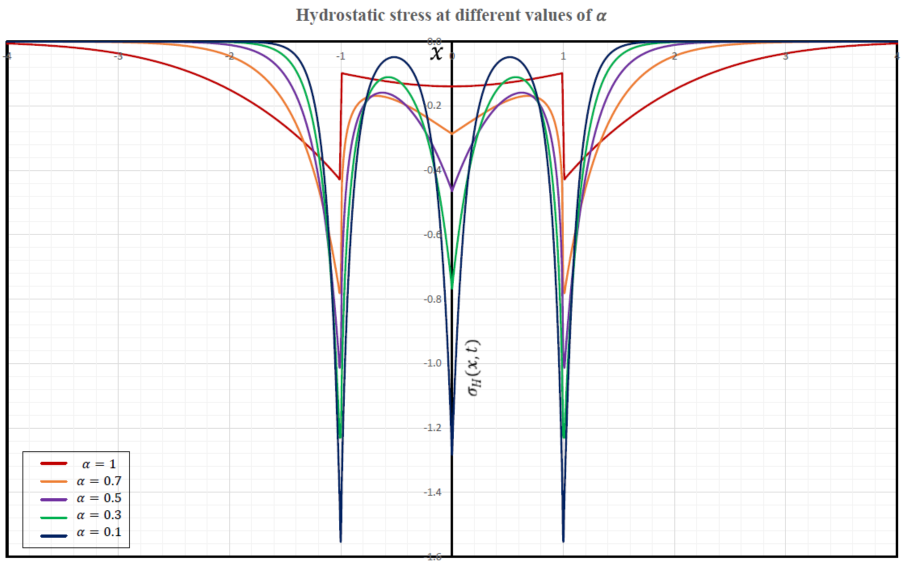

Fig. 5. The distribution of hydrostatic stress represented for various values of the fractional parameter α, illustrating the influence of anomalous thermal conductivity on the stress response

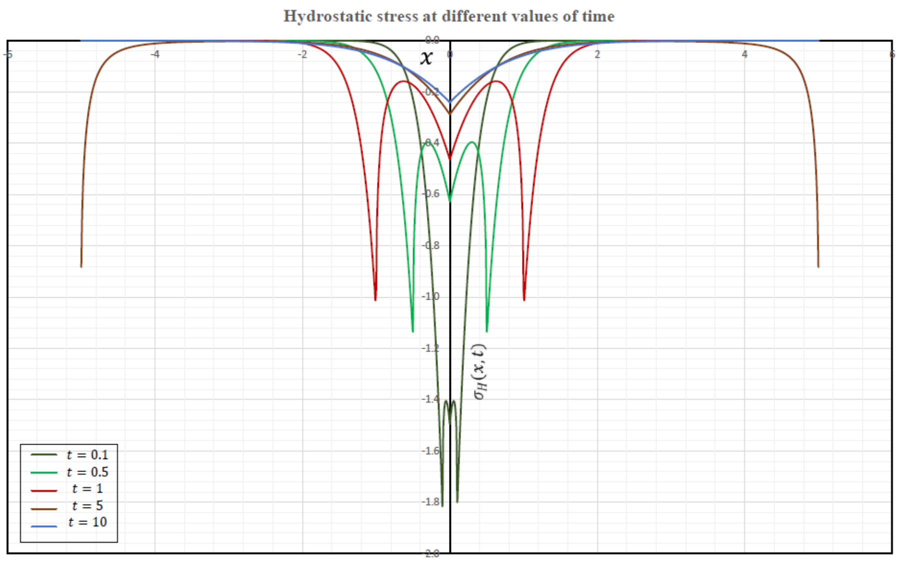

Fig. 6. The variation of hydrostatic stress presented for different time instances t, showing the temporal evolution of the stress field

Conclusions

The interaction between electromagnetic fields and fractional-order thermoelasticity in unbounded domains was studied. By incorporating Maxwell's equations into the governing system and applying Laplace and Fourier transforms, the uncoupled equations for temperature and displacement are solved analytically. The analysis reveals the finite-speed propagation of thermal and mechanical waves and highlights the effects of material parameters on the system's response. Analytical techniques are employed to solve the system, revealing that the electromagnetic effects do not significantly influence the temperature.

CRediT authorship contribution statement

Noha Samir: writing – original draft, investigation, data curation; **Mohamed A. Abdou**: writing – review & editing, supervision, data curation; **Emad Awad**: conceptualization, supervision, writing – review & editing, investigation.

Conflict of interest

The authors declare that they have no conflict of interest.

References

1. Biot MA. Thermoelasticity and irreversible thermodynamics. *Journal of Applied Physics.* 1956;27(3): 240–253.
2. Povstenko YZ. Fractional heat conduction equation and associated thermal stress. *Journal of Thermal Stresses.* 2005;28(1): 83–102.
3. Samir N, Abdou MA, Awad E. On the quasi-static theory of space-time fractional thermoelasticity in the unbounded domains. *Faculty of Education Journal Alexandria University.* 2024;34(4): 313–349.
4. Rukolaine SA. Hyperbolicity of the ballistic-conductive model of heat conduction: the reverse side of the coin. *Zeitschrift für angewandte Mathematik und Physik.* 2024;75(2): 50.
5. Rukolaine S. Effects observed in the ballistic-conductive model of heat conduction. *St. Petersburg State Polytechnical University Journal. Physics and Mathematics.* 2023;16(1.2): 315–321.
6. Sobolev SL. Nonlocal two-temperature model: Application to heat transport in metals irradiated by ultrashort laser pulses. *International Journal of Heat and Mass Transfer.* 2016;94: 138–144.
7. Sobolev SL, Kudinov IV. Dispersion relation and frequency-dependent thermal conductivity of the two-temperature systems. *International Journal of Thermal Sciences.* 2025;214: 109937.
8. Awad E, Dai W, Sobolev S. Thermal oscillations and resonance in electron–phonon interaction process. *Zeitschrift für angewandte Mathematik und Physik.* 2024;75(4): 143.
9. Bassiouny E. Hyperbolic two temperature fractional order one dimensional thermoelastic model heated by a pulse of laser. *Materials Physics and Mechanics.* 2020;44(1): 66–76.
10. Kumar R, Vohra R. Steady state response due to moving load in thermoelastic material with double porosity. *Materials Physics and Mechanics.* 2020;44(2): 172–185.
11. Levi GY, Igumnov L. Some properties of the thermoelastic prestressed medium Green function. *Materials Physics and Mechanics.* 2015;23(1): 42–46.
12. Griffiths DJ. *Introduction to electrodynamics.* Cambridge University Press; 2023.
13. Doria R, Mendes LS. Four–Four Maxwell equations. *Modern Physics Letters A.* 2023;38(22n23): 2350106.
14. Jackson JD. *Classical electrodynamics.* John Wiley & Sons; 2021.
15. Ramzan M, Gul H, Mursaleen M, Nisar KS, Jamshed W, Muhammad T. Von Karman rotating nanofluid flow with modified Fourier law and variable characteristics in liquid and gas scenarios. *Scientific Reports.* 2021;11(1): 16442.
16. Awad E. Modeling of anomalous thermal conduction in thermoelectric magnetohydrodynamics: Couette formulation with a multiphase pressure gradient. *Physics of Fluids.* 2024;36(3): 033608.

17. Awad E, Samir N. A closed-form solution for thermally induced affine deformation in unbounded domains with a temporally accelerated anomalous thermal conductivity. *Journal of Physics A: Mathematical and Theoretical.* 2024;57(45): 455202.
18. Awad E, Metzler R. Crossover dynamics from superdiffusion to subdiffusion: Models and solutions. *Fractional Calculus and Applied Analysis.* 2020;23(1): 55–102.
19. Barrios-Piña H, Viazzo S, Rey C. Total energy balance in a natural convection flow. *International Journal of Numerical Methods for Heat & Fluid Flow.* 2017;27(8): 1735–1747.
20. Saichev AI, Zaslavsky GM. Fractional kinetic equations: solutions and applications. *Chaos: An Interdisciplinary Journal of Nonlinear Science.* 1997;7(4): 753–764.
21. Mainardi F, Luchko Y, Pagnini G. The fundamental solution of the space-time fractional diffusion equation. ArXiv [Preprint] 2007. Available from: doi.org/10.48550/arXiv.cond-mat/0702419.
22. Gorenflo R, Mainardi F. Fractional Calculus. In: Carpinteri A, Mainardi F. (eds.) *Fractals and Fractional Calculus in Continuum Mechanics*. Vienna: Springer; 1997. p.223–276.
23. Sandev T, Tomovski Z. *Fractional equations and models: theory and applications.* Cham, Switzerland: Springer; 2019.
24. Awad E, Sandev T, Metzler R, Chechkin A. Closed-form multi-dimensional solutions and asymptotic behaviors for subdiffusive processes with crossovers: I. Retarding case. *Chaos, Solitons & Fractals.* 2021;152: 111357.
25. Nowacki W. *Thermoelasticity.* Elsevier; 2013.
26. Fayik M, El Dhaba A, Awad E. Diffusion-induced stresses due to an impulsive mass source under non-Fickian mass transfer models. *Materials Physics and Mechanics.* 2023;51(1): 93–107.
27. Mainardi F, Mura A, Pagnini G. The M-Wright Function in Time-Fractional Diffusion Processes: A Tutorial Survey. *International Journal of Differential Equations.* 2010;2010(1): 104505.
28. Garra R, Garrappa R. The Prabhakar or three parameter Mittag–Leffler function: Theory and application. *Communications in Nonlinear Science and Numerical Simulation.* 2018;56: 314–329.
29. Mathai AM, Saxena RK, Haubold HJ. *The H-function: theory and applications*. Springer; 2009.
30. Awad E. Dual-Phase-Lag in the balance: Sufficiency bounds for the class of Jeffreys' equations to furnish physical solutions. *International Journal of Heat and Mass Transfer.* 2020;158: 119742.